Letter

Thouless energy across the many-body localization transition in Floquet systems

Michael Sonner,[1] Maksym Serbyn,[2] Zlatko Papić,[3] and Dmitry A. Abanin[1]
[1]*Department of Theoretical Physics, University of Geneva, 24 quai Ernest-Ansermet, 1211 Geneva, Switzerland*
[2]*IST Austria, Am Campus 1, 3400 Klosterneuburg, Austria*
[3]*School of Physics and Astronomy, University of Leeds, Leeds LS2 9JT, United Kingdom*

(Received 12 June 2021; accepted 26 July 2021; published 26 August 2021)

The notion of Thouless energy plays a central role in the theory of Anderson localization. We investigate and compare the scaling of Thouless energy across the many-body localization (MBL) transition in a Floquet model. We use a combination of methods that are reliable on the ergodic side of the transition (e.g., spectral form factor) and methods that work on the MBL side (e.g., typical matrix elements of local operators) to obtain a complete picture of the Thouless energy behavior across the transition. On the ergodic side, Thouless energy decreases slowly with the system size, while at the transition it becomes comparable to the level spacing. Different probes yield consistent estimates of Thouless energy in their overlapping regime of applicability, giving the location of the transition point nearly free of finite-size drift. This work establishes a connection between different definitions of Thouless energy in a many-body setting and yields insights into the MBL transition in Floquet systems.

DOI: 10.1103/PhysRevB.104.L081112

Introduction. Out-of-equilibrium properties of disordered interacting systems have recently attracted much interest. This attention is due to the remarkable fact that such systems may avoid thermalization via the phenomenon of many-body localization (MBL) [1–4]. The characteristic features of MBL, apart from the system's long-term memory of the initial state, include logarithmic spreading of entanglement [5,6] and emergent integrability [7,8], which is stable with respect to finite, but sufficiently weak, generic local perturbations. The last property implies that MBL systems represent a paradigm of nonthermal phases of matter, which violate the eigenstate thermalization hypothesis [9–11] at a finite energy density above the ground state.

In addition to stability with respect to perturbations of the Hamiltonian, pioneering works [12–17] have demonstrated the existence of MBL in the presence of periodic driving. In these Floquet systems, MBL allows us to avoid unbounded heating, thus enabling the existence of new nonequilibrium phases of matter, such as time crystals [18,19] and anomalous Floquet insulators [20,21]. These and related phases are actively investigated in current experiments with nitrogen vacancy centers [22,23], cold atoms [24], and trapped ions [25].

Despite significant recent progress, many open questions remain in the field of MBL, such as the transition between MBL and the delocalized (thermalizing) phase. In studies of localization-delocalization transitions in *single-particle* systems [26,27], a central role is played by the so-called Thouless energy E_{Th} [28]. Intuitively, E_{Th} sets the scale at which the system's energy levels develop random-matrix-like correlations. On the one hand, E_{Th} is directly linked to a physical observable, the system's conductance, while on the other hand, E_{Th} can be defined and practically computed by the response of energy levels to the twisting of boundary conditions. Linking seemingly unrelated characteristics of the system, E_{Th} underlies the celebrated scaling theory of localization [29].

The central role of E_{Th} in the understanding of single-particle localization has motivated its recent extensions to many-body systems. In particular, Ref. [30] introduced a probe based on the behavior of typical matrix elements of local operators, while Refs. [31–34] used spectral properties such as fluctuations of the level number and spectral form factor to map out E_{Th} as a function of disorder strength. References [35,36], following the original Thouless idea, investigated the sensitivity of many-body energy levels to boundary conditions. Furthermore, the behavior of the spectral function was used as yet another probe of E_{Th} [37]. The inverse of E_{Th}, the Thouless time, can be understood as a characteristic timescale of the system's dynamics [38]. It is worth noting that E_{Th} is also one of the central building blocks of phenomenological renormalization group studies of MBL-thermal transition [39,40]. Thus, several candidates for the generalization of E_{Th} to disordered interacting systems have been proposed. However, the comparison of different definitions of E_{Th} is currently missing. Moreover, in Hamiltonian systems, the interpretation of E_{Th} behavior is often complicated by pronounced finite-size effects and nonuniform density of states [41].

The goal of this paper is to compare the behavior of different notions of E_{Th} in many-body systems. Following Ref. [15], we study a many-body Floquet model without any conservation laws, which reduces finite-size effects compared to the more often studied Hamiltonian models, such as the disordered XXZ spin chain [42]. An additional advantage of the Floquet model is that the many-body density of states is uniform, thus removing the need for spectral unfolding [43]. In Hamiltonian models of MBL, on the other hand, the density

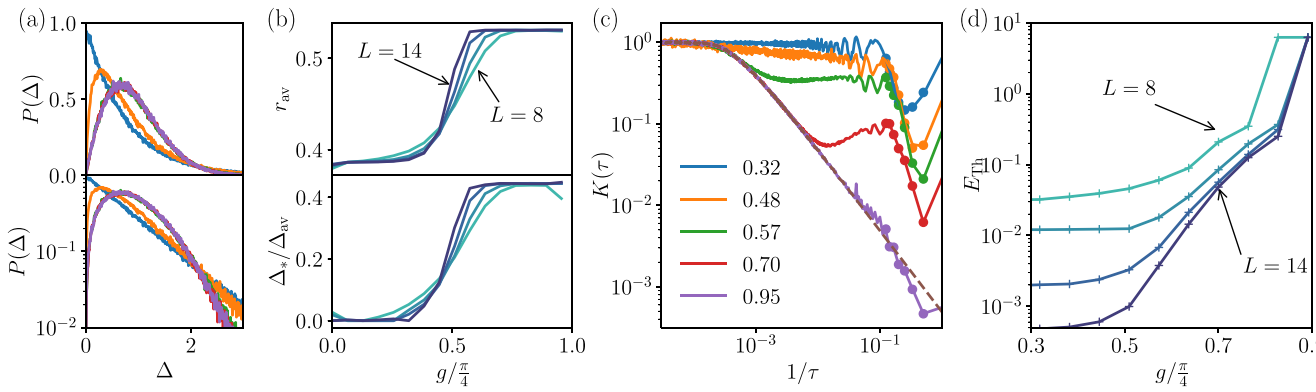

FIG. 1. Spectral properties across the MBL transition. (a) Level spacing distribution for different values of disorder $g/\frac{\pi}{4}$; see legend in (c). The curves for the three most ergodic values overlap. (b) Average ratio of adjacent level spacings $r_{\rm av}$ and the most likely level spacing value Δ_* interpolate between different limiting values in the MBL and ergodic phases. Different curves are for system sizes $L = 8, \ldots, 14$, and their crossing yields an estimate for the location of MBL transition $g_* \approx 0.36$. (c) Deviation of the spectral form factor $K(\tau)$ from the random matrix prediction (dashed line) occurs at progressively larger values of $1/\tau$ as disorder strength is decreased (g increases). Data shown for $L = 12$ and the values of $g/\frac{\pi}{4}$ are specified in the legend. Dots indicate the data points obtained with exact disorder averaging using a dual transfer matrix approach [46–48]. (d) $E_{\rm Th}$ defined as $1/\tau$ at the point of deviation of $K(\tau)$ from the random matrix curve in (c). $E_{\rm Th}$ exhibits a slow decrease with L on the ergodic side, while in the transition region $E_{\rm Th}$ decreases exponentially with L.

of states varies strongly with energy; in particular, states at the edge of the spectrum are more localized than those in the center, leading to the many-body mobility edge [30,44,45].

Below we demonstrate that a number of different definitions of $E_{\rm Th}$ are qualitatively consistent across the MBL transition in the Floquet model defined in Eq. (1). At weak disorder we find that $E_{\rm Th}$ slowly decreases with system size, consistent with recent analytical results obtained in the large-N limit, where the scaling $E_{\rm Th}(L) \propto 1/\ln L$ was found [32]. $E_{\rm Th}$ decreases upon approaching the MBL transition, becoming smaller than the many-body level spacing. Spectral probes naturally operate in one of the two regimes: (i) the ergodic regime, where $E_{\rm Th}$ is large, and (ii) the transition regime and MBL phase, where $E_{\rm Th}$ is comparable to or smaller than level spacing. In contrast, the statistics of matrix elements allows us to access both regimes.

Model. We consider the following Floquet model for a periodic chain of L spins $1/2$, defined by the evolution operator over one driving period:

$$\hat{F} = \exp\left[-i\sum_j g\sigma_j^x\right]\exp\left[-i\sum_j \left(J\sigma_j^z\sigma_{j+1}^z + h_j\sigma_j^z\right)\right], \quad (1)$$

where σ_j^α, $\alpha = x, y, z$ are the Pauli operators and $h_j \in [0, 2\pi]$ are uniformly distributed random variables. The parameters g and J determine the importance of disorder in the system. Here, we fix $J = g$ and vary g from zero, where the model is trivially localized, to $\pi/4$, where the model (1) becomes "perfectly ergodic" [46,47,49]; in particular, it exactly follows certain predictions of random-matrix theory [47]. Furthermore, Refs. [15,17] studied a similar Floquet model, with the fields h_j having both constant and random components; in contrast, in our model h_j are fully random.

In order to study the phase diagram of the model (1) and compare different probes of $E_{\rm Th}$ we use exact diagonalization. We numerically calculate [50] the quasienergies θ_n (defined modulo 2π) and eigenvectors $|n\rangle$ of the Floquet operator, which satisfy $\hat{F}|n\rangle = e^{i\theta_n}|n\rangle$. We first extract $E_{\rm Th}$ from spectral probes which include the level statistics and spectral form factor. Afterwards, we proceed with the statistics of matrix elements of local operators, which allows us to extract $E_{\rm Th}$ using typical matrix elements and spectral functions.

Level statistics. The statistics of (quasi)energy levels has long been used as a probe of quantum chaos and integrability in single-particle systems [51], and in recent years it has been fruitfully applied in a many-body setting. It is worth noting that spectral probes may reveal the breakdown of chaos and ergodicity even when conservation laws are not known explicitly. The MBL phase, owing to the emergence of local integrals of motion, exhibits Poisson level statistics, while the ergodic phase is characterized by level repulsion following Wigner-Dyson random-matrix level statistics [42]. Due to the form of the Floquet operator in Eq. (1), the relevant random matrix theory ensemble is the circular orthogonal ensemble (COE) [43]. These limiting cases of level statistics for the model (1) are demonstrated in Fig. 1(a), which shows the probability distribution of level spacings $P(\Delta)$, where the level spacing is defined as $\Delta_n = (\theta_{n+1} - \theta_n)/\delta_{\rm av}$, with $\delta_{\rm av} = 2\pi/2^L$. This definition implies that $\langle\Delta\rangle = 1$, and no unfolding is needed due to the constant density of states.

At small values of $g \lesssim 0.3$ corresponding to strong disorder, the distribution of level spacings $P(\Delta)$ is Poissonian, signaling an MBL phase. At large values of g, when the system is deeply in the ergodic phase, $P(\Delta)$ is described by the COE ensemble. At intermediate values of g, level repulsion is still present, as evidenced by the vanishing of $P(\Delta)$ as $\Delta \to 0$. However, the maximum Δ_* of $P(\Delta)$ decreases as g is decreased, compared to the random-matrix value. This corresponds to the breakdown of the random-matrix description and weakening of the level repulsion in the critical region, which is also reflected in the softer-than-Gaussian tail of $P(\Delta)$ at large Δ [see the bottom panel in Fig. 1(a)].

To estimate the location of the MBL-thermal transition from level statistics, we first use the r parameter [52],

defined as $r_{\rm av} = \langle \min(\Delta_n, \Delta_{n+1})/\max(\Delta_n, \Delta_{n+1})\rangle$, where $\langle\cdots\rangle$ denotes averaging over the spectrum and different disorder realizations. For the Poisson distribution, this parameter has the value $r_{\rm av} \approx 0.39$, while for the COE-distributed levels it equals $r_{\rm av} \approx 0.54$ [53]. The behavior of the $r_{\rm av}$ parameter for different system sizes is illustrated in Fig. 1(b). The curves, interpolating between the Poisson and COE values at small and large g, respectively, cross at $g_* \approx 0.36$, which we take as the location of the critical point separating MBL and thermal phases. We note that the drift of the crossing point with increasing L, which is pronounced in Hamiltonian models, appears to be nearly absent for our model, which we attribute to the absence of conservation laws [15].

An alternative way of estimating the location of the critical point is by studying the most likely value of Δ_*, defined by the maximum of $P(\Delta)$. The parameter Δ_* is expected to interpolate between zero in the MBL phase and the COE value of $\approx$0.45 in the ergodic phase. Thus, its finite-size behavior provides a probe of the critical region. Indeed, different curves in Fig. 1(b) cross at a value consistent with that estimated from the r parameter above.

Spectral form factor. The spectral form factor (SFF) probes spectral correlations at energy scales larger than the average level spacing [54]. SFF is given by the Fourier transform of the two-level correlation function at "time" $\tau > 0$,

$$K(\tau) = \langle |{\rm tr}(\hat{F}^\tau)|^2\rangle = \left\langle \sum_{n,m} e^{i\tau(\theta_n - \theta_m)} \right\rangle, \tag{2}$$

where $\hat{F}$ is the Floquet operator (1) and $\langle\cdots\rangle$ denotes disorder averaging. As mentioned above, in our Floquet model there is no need for spectral unfolding, which is necessary for Hamiltonian models. Further, given that quasienergies are defined modulo 2π, we take τ to be a positive integer. Intuitively, SFF at time τ probes spectral repulsion or its absence at the quasienergy scale $\sim 1/\tau$.

Random-matrix theory [43] predicts a linear dependence of SFF on τ. Ergodic systems are expected to exhibit such linear behavior $K(\tau) \propto |\tau|$ at energy scales below $E_{\rm Th}$, $1/\tau \lesssim E_{\rm Th}$. Thus, SFF provides a way to extract $E_{\rm Th}$; however, such extraction is possible only in the ergodic phase, where $E_{\rm Th}$ is large, while in the MBL phase other means should be sought. We note that at energy scales much smaller than the average level spacing, $1/\tau \ll \delta_{\rm av}$, the SFF becomes a constant, irrespective of whether the system is ergodic.

We computed SFF in two complementary ways: first, by directly evaluating Eq. (2) from the quasienergy spectrum and averaging over 100–1000 disorder configurations and, second, by using the exactly disorder averaged dual transfer matrix approach described in Refs. [46–48,55]. The latter method is limited to relatively short times $\tau \sim 10$ but provides a useful benchmark for confirming that the disorder averaging in the former method is sufficient.

Figure 1(c) shows that in the ergodic phase ($g \gtrsim g_*$), SFF depends linearly on τ up to $E_{\rm Th}(g, L)$, as predicted by random matrix theory. The scaling of $E_{\rm Th}$ for different system sizes, shown in Fig. 1(d), reveals a slow decrease of $E_{\rm Th}(g, L)$ with L. This result is consistent with previous results [32] obtained for a model of q-state spins with $q \to \infty$, as well as with general arguments based on the dual transfer matrix approach [55]. In the critical region, we find the scaling $E_{\rm Th}(g, L) \propto \delta_{\rm av}$, showing that, similar to Hamiltonian systems, at the MBL-thermal transition the ratio of $E_{\rm Th}$ and level spacing remains approximately constant [30]. Note that the point where $E_{\rm Th}$ extracted from SFF exhibits clear exponential scaling with L coincides with the point where Δ_* remains constant [Figs. 1(b) and 1(d)], demonstrating that the two probes yield consistent results.

Matrix elements. An attractive feature of spectral probes is their universality: additional conservation laws, irrespective of their precise form, would lead to Poisson level statistics. However, to describe real-time behavior of physical observables and to obtain insights into the structure of conservation laws in nonthermalizing phases, it is necessary to study the structure of eigenfunctions and matrix elements of physical operators. Numerically, this comes with an added advantage of utilizing more information per sample. Below we will investigate two ways of extracting $E_{\rm Th}$ from matrix elements of local operators which have been employed in Hamiltonian models of MBL: the ratio between the matrix elements and level spacing [30] and spectral functions [37,56].

We first focus on the statistics of matrix elements of a local operator $\hat{O}$ between the Floquet eigenstates, $O_{nm} = |\langle n|\hat{O}|m\rangle|$, and the corresponding "many-body Thouless parameter" defined here as $\mathcal{G} = [O_{nm}/\delta_{\rm av}]_*$. The notation $[\cdots]_*$ denotes the mode value, a definition that is nearly identical to the one that uses an average of the logarithm [30,50]. Deep in the ergodic phase, matrix elements obey the eigenstate thermalization hypothesis (ETH) [9,10], which implies scaling $O_{nm} \propto \sqrt{\delta_{\rm av}} R_{nm}$, where R_{nm} are random, normal-distributed numbers with a variance of order 1. This corresponds to $\mathcal{G} \propto \delta_{\rm av}^{-1/2} \gg 1$. In the MBL phase, in contrast, owing to the emergence of local integrals of motion, typical matrix elements decay much faster than the level spacing $\mathcal{G}(L) \propto 2^{-\kappa L}$, with $\kappa > 1$. Further, similar to localized wave functions, the matrix elements develop a broad, lognormal distribution [27].

We studied several local operators for the model in Eq. (1), and the resulting distribution for the operator $\hat{S}^z = \sigma_1^z/2$ is illustrated in Figs. 2(a)–2(c). As expected, we observe that in the MBL phase the distribution $P(S^z_{nm}/\delta_{\rm av})$ is lognormal, and the mode of $S^z_{nm}/\delta_{\rm av}$ decreases exponentially with L. On the ergodic side, in contrast, this ratio exponentially increases, as predicted by ETH, while the distribution remains narrow. In the critical region, we find that the distribution broadens, while the typical ratio $P(S^z_{nm}/\delta_{\rm av})$ remains approximately independent of L.

The behavior of $\mathcal{G}$ in Fig. 2(d) serves as an indicator of the location of transition, which yields an estimate consistent with spectral probes. Similar to the finite-size scaling of $r_{\rm av}$, we do not find any significant drift of the crossing point. An interesting question concerns the relation of $\mathcal{G}$ and Δ_*. We find that on the MBL side of the transition, $\mathcal{G}(L)$ decays much faster than the latter quantity. We attribute this to the fact that $\mathcal{G}$ probes matrix elements between eigenstates with a quasienergy difference of order 1, while Δ_*, rather, probes matrix elements between nearby energy states, which are enhanced.

In order to obtain the critical exponents, we perform the scaling collapse of $\mathcal{G}(L)$ shown in Fig. 2(e). The value of the

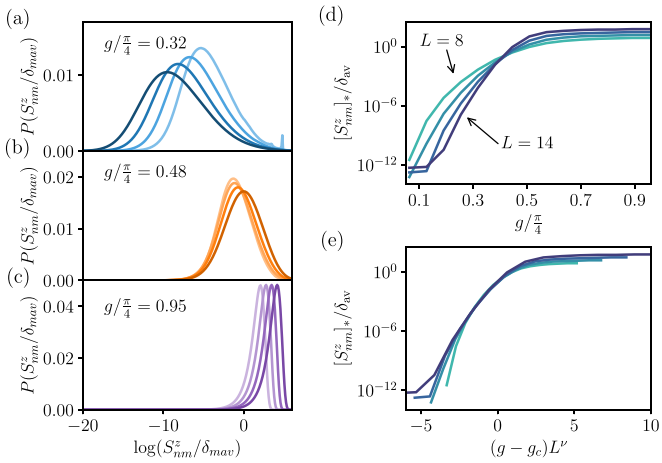

FIG. 2. (a)–(c) Statistics of ratios between matrix elements and level spacing display qualitatively different behavior in different phases. Color corresponds to system sizes $L = 8, \ldots, 14$ in order of increasing intensity. (a) In the MBL phase the distribution broadens, and the typical value decreases exponentially with system size. (b) At the transition, the mode moves very little, but the distribution broadens with L. (c) Deep in the ergodic phase, the evolution of the distribution is consistent with ETH predictions. (d) Mode of the matrix element distribution vs g. The crossing point of curves for different L is consistent with the transition estimate from spectral probes. (e) Scaling collapse of the data in (d) gives the critical exponent $\nu \approx 1.2$.

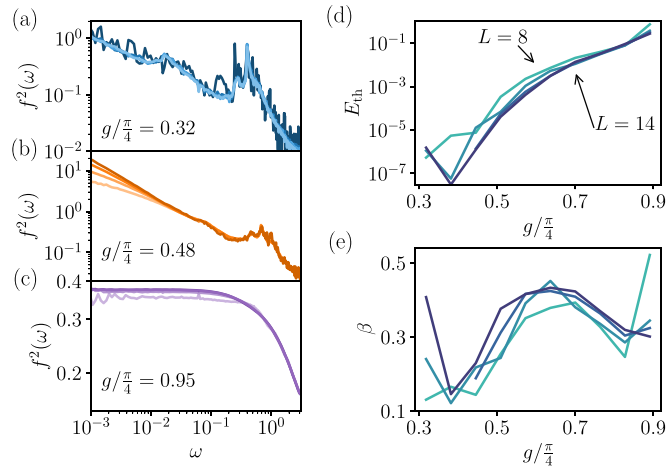

FIG. 3. Spectral function (3) for different system sizes (a) in the MBL phase, (b) at the transition, and (c) in the fully ergodic phase. For energies larger than $E_{\rm Th}$ the spectral function does not depend on system size. Since $E_{\rm Th}$ is very small on the MBL side and constant in the ergodic phase, the spectral function collapses in the full range of considered frequencies. (d) Scaling of $E_{\rm Th}$ extracted from the kww fit to the spectral function [50]. (e) Exponent of the asymptotic power law of the kww fit [59].

critical exponent is $\nu \approx 1.2$, which still violates the Harris criterion [57,58]; however, this violation is weaker than the exponent in Hamiltonian systems [44]. Weaker violation of the Harris criterion, along with the almost absent drift of the crossing point, suggests weaker finite-size effects due to the absence of conserved quantities.

Spectral function. The spectral function (SF) quantifies the energy structure of a matrix element which can be experimentally probed in absorption spectroscopy. The SF of an operator $\hat{O}$ is defined as

$$f^2(\omega) = 2^{-L} \sum_{n,m} |\langle n|\hat{O}|m\rangle|^2 \delta(\omega - \theta_n + \theta_m), \qquad (3)$$

where the sum runs over all eigenstates, corresponding to the infinite-temperature ensemble. This SF is a Fourier transform of the infinite-temperature real-time correlation function $\langle \hat{O}(t)\hat{O}(0)\rangle_{T=\infty}$; thus, it contains information about the system's dynamical timescales. In particular, in the ergodic phase, the spectral function has a plateau for $\omega \lesssim E_{\rm Th}$ since the Thouless time is a scale at which the excitations have propagated through the system and the dynamics have saturated.

The evolution of the disorder-averaged spectral function of the $\hat{S}^z$ operator $f^2(\omega)$ across the MBL-thermal transition is illustrated in Figs. 3(a)–3(c). Deep in the MBL phase, the spectral function develops a δ-function peak at $\omega = 0$ [50], while its behavior at $\omega > 0$ approximately follows power-law behavior, also observed in Hamiltonian MBL systems [37]. In the critical region, a power law with a larger exponent gradually develops, and the spectral function does not exhibit a visible plateau, consistent with $E_{\rm Th}$ becoming of the order of the level spacing. Deep in the ergodic phase [Fig. 3(c)], in contrast, the spectral function shows a wide plateau, which yields an estimate of $E_{\rm Th}$ that is qualitatively consistent with spectral probes.

To quantify $E_{\rm Th}$ from the spectral function we fit $f^2(\omega)$ using the Fourier transform of a stretched exponential (the so-called kww function [59]), which is consistent with recent work [17] that reported the stretched exponential decay of real-time correlation functions. The fitting procedure [50] results in $E_{\rm Th}$ shown in Fig. 3(d). The exponent β, which controls the asymptotic power-law behavior of the spectral function, is illustrated in Fig. 3(e). The spectral function $f^2(\omega)$ behaves as $1/\omega^{1+\beta}$ for $\omega \gg E_{\rm Th}$. We note that β exhibits nonmonotonic behavior with the maximum around the transition point. Additionally, in the vicinity of the transition, we observe a collapse of the spectral function $f^2(\omega)/2^L$ plotted as a function of $\omega/\delta_{\rm av}$ for different system sizes [50].

Discussion. We have studied and compared the behavior of $E_{\rm Th}$ across the Floquet many-body localization transition obtained using various probes based on spectral properties and matrix elements of local observables. Among the considered probes, the SFF and spectral function work well on the ergodic side, yielding consistent values of $E_{\rm Th}$ that decrease slowly with L. Such behavior is in contrast to the Hamiltonian models, where $E_{\rm Th}(L) \propto L^{-1/\gamma}$ exhibits subdiffusive scaling with L with a disorder-dependent exponent [60]. In the critical region, $E_{\rm Th}$ becomes of the order of many-body level spacing. In the critical region the extraction of $E_{\rm Th}$ from the SFF and spectral function becomes unreliable, and we obtain $E_{\rm Th}$ from the most probable value of the level spacing and many-body Thouless parameter.

In addition to scrutinizing different notions of $E_{\rm Th}$, our work provides insights into the MBL transition in the Floquet

model. The absence of any conserved quantities in the considered model reduces the finite-size effects, which is manifested in the larger value of the critical exponent and weaker drift of the critical point, in agreement with earlier numerical studies of a different model using a different set of probes [15]. Moreover, we find the properties of spectral functions to be consistent with the stretched exponential relaxation of real-time correlation functions [17].

Several open questions remain for future work. In particular, in light of the apparent absence of subdiffusion in the ergodic phase in Floquet models, it would be interesting to investigate the rare-region effects on the spreading of entanglement, correlation function decay, and implications for the nature of the transition into the MBL phase. Furthermore, the link between different definitions of E_{Th} established here may serve as a foundation for developing a scaling theory of the Floquet-MBL transition.

Note added in proof. Recently, Ref. [61] investigated SFF in a Floquet model of MBL using the dual disorder-averaged transfer matrix approach employed above.

In accordance with the EPSRC policy framework on research data, this publication is theoretical work that does not require supporting research data.

Acknowledgments. We thank S. Garratt for useful comments on the manuscript. This work was supported by the Swiss National Science Foundation (M. Sonner and D.A.A.) and by the European Research Council (ERC) under the European Union's Horizon 2020 research and innovation program (M. Serbyn, Grant Agreement No. 850899, and D.A.A., Grant Agreement No. 864597). Z.P. acknowledges support from EPSRC Grant No. EP/R020612/1 and from Leverhulme Trust Research Leadership Award No. RL-2019-015. The computations were performed on the Baobab cluster of the University of Geneva.

[1] E. Altman and R. Vosk, Universal dynamics and renormalization in many-body-localized systems, Annu. Rev. Condens. Matter Phys. **6**, 383 (2015).

[2] R. Nandkishore and D. A. Huse, Many-body localization and thermalization in quantum statistical mechanics, Annu. Rev. Condens. Matter Phys. **6**, 15 (2015).

[3] D. A. Abanin, E. Altman, I. Bloch, and M. Serbyn, Colloquium: Many-body localization, thermalization, and entanglement, Rev. Mod. Phys. **91**, 021001 (2019).

[4] F. Alet and N. Laflorencie, Many-body localization: An introduction and selected topics, C. R. Phys. **19**, 498 (2018).

[5] M. Znidaric, T. Prosen, and P. Prelovsek, Many-body localization in the Heisenberg XXZ magnet in a random field, Phys. Rev. B **77**, 064426 (2008).

[6] J. H. Bardarson, F. Pollmann, and J. E. Moore, Unbounded Growth of Entanglement in Models of Many-Body Localization, Phys. Rev. Lett. **109**, 017202 (2012).

[7] M. Serbyn, Z. Papić, and D. A. Abanin, Local Conservation Laws and the Structure of the Many-Body Localized States, Phys. Rev. Lett. **111**, 127201 (2013).

[8] D. A. Huse, R. Nandkishore, and V. Oganesyan, Phenomenology of fully many-body-localized systems, Phys. Rev. B **90**, 174202 (2014).

[9] J. M. Deutsch, Quantum statistical mechanics in a closed system, Phys. Rev. A **43**, 2046 (1991).

[10] M. Srednicki, Chaos and quantum thermalization, Phys. Rev. E **50**, 888 (1994).

[11] M. Rigol, V. Dunjko, and M. Olshanii, Thermalization and its mechanism for generic isolated quantum systems, Nature (London) **452**, 854 (2008).

[12] A. Lazarides, A. Das, and R. Moessner, Fate of Many-Body Localization under Periodic Driving, Phys. Rev. Lett. **115**, 030402 (2015).

[13] P. Ponte, Z. Papić, F. Huveneers, and D. A. Abanin, Many-Body Localization in Periodically Driven Systems, Phys. Rev. Lett. **114**, 140401 (2015).

[14] D. A. Abanin, W. De Roeck, and F. Huveneers, Theory of many-body localization in periodically driven systems, Ann. Phys. **372**, 1 (2016).

[15] L. Zhang, V. Khemani, and D. A. Huse, A Floquet model for the many-body localization transition, Phys. Rev. B **94**, 224202 (2016).

[16] C. Sünderhauf, D. Pérez-García, D. A. Huse, N. Schuch, and J. I. Cirac, Localization with random time-periodic quantum circuits, Phys. Rev. B **98**, 134204 (2018).

[17] T. L. M. Lezama, S. Bera, and J. H. Bardarson, Apparent slow dynamics in the ergodic phase of a driven many-body localized system without extensive conserved quantities, Phys. Rev. B **99**, 161106(R) (2019).

[18] V. Khemani, A. Lazarides, R. Moessner, and S. L. Sondhi, Phase Structure of Driven Quantum Systems, Phys. Rev. Lett. **116**, 250401 (2016).

[19] D.V. Else, B. Bauer, and C. Nayak, Floquet Time Crystals, Phys. Rev. Lett. **117**, 090402 (2016).

[20] H. C. Po, L. Fidkowski, T. Morimoto, A. C. Potter, and A. Vishwanath, Chiral Floquet Phases of Many-Body Localized Bosons, Phys. Rev. X **6**, 041070 (2016).

[21] F. Nathan, D. Abanin, E. Berg, N. H. Lindner, and M. S. Rudner, Anomalous Floquet insulators, Phys. Rev. B **99**, 195133 (2019).

[22] S. Choi, J. Choi, R. Landig, G. Kucsko, H. Zhou, J. Isoya, F. Jelezko, S. Onoda, H. Sumiya, V. Khemani, C. von Keyserlingk, N. Y. Yao, E. Demler, and M. D. Lukin, Observation of discrete time-crystalline order in a disordered dipolar many-body system, Nature (London) **543**, 221 (2017).

[23] J. Choi, H. Zhou, S. Choi, R. Landig, W. W. Ho, J. Isoya, F. Jelezko, S. Onoda, H. Sumiya, D. A. Abanin, and M. D. Lukin, Probing Quantum Thermalization of a Disordered Dipolar Spin Ensemble with Discrete Time-Crystalline Order, Phys. Rev. Lett. **122**, 043603 (2019).

[24] P. Bordia, H. Lüschen, U. Schneider, M. Knap, and I. Bloch, Periodically driving a many-body localized quantum system, Nat. Phys. **13**, 460 (2017).

[25] J. Zhang, P. W. Hess, A. Kyprianidis, P. Becker, A. Lee, J. Smith, G. Pagano, I. D. Potirniche, A. C. Potter, A. Vishwanath, N. Y. Yao, and C. Monroe, Observation of a discrete time crystal, Nature (London) **543**, 217 (2017).

[26] B. Kramer and A. MacKinnon, Localization: Theory and experiment, Rep. Prog. Phys. **56**, 1469 (1993).
[27] F. Evers and A. D. Mirlin, Anderson Transitions, Rev. Mod. Phys. **80**, 1355 (2008).
[28] J. T. Edwards and D. J. Thouless, Numerical studies of localization in disordered systems, J. Phys. C **5**, 807 (1972).
[29] E. Abrahams, P. W. Anderson, D. C. Licciardello, and T. V. Ramakrishnan, Scaling Theory of Localization: Absence of Quantum Diffusion in Two Dimensions, Phys. Rev. Lett. **42**, 673 (1979).
[30] M. Serbyn, Z. Papić, and D. A. Abanin, Criterion for Many-Body Localization-Delocalization Phase Transition, Phys. Rev. X **5**, 041047 (2015).
[31] C. L. Bertrand and A. M. García-García, Anomalous Thouless energy and critical statistics on the metallic side of the many-body localization transition, Phys. Rev. B **94**, 144201 (2016).
[32] A. Chan, A. De Luca, and J. T. Chalker, Spectral Statistics in Spatially Extended Chaotic Quantum Many-Body Systems, Phys. Rev. Lett. **121**, 060601 (2018).
[33] A. Prakash, J. H. Pixley, and M. Kulkarni, The universal spectral form factor for many-body localization, Phys. Rev. Research **3**, L012019 (2021).
[34] P. Sierant, D. Delande, and J. Zakrzewski, Thouless Time Analysis of Anderson and Many-Body Localization Transitions, Phys. Rev. Lett. **124**, 186601 (2020).
[35] M. Filippone, P. W. Brouwer, J. Eisert, and F. von Oppen, Drude weight fluctuations in many-body localized systems, Phys. Rev. B **94**, 201112(R) (2016).
[36] C. Monthus, Many-body-localization transition: sensitivity to twisted boundary conditions, J. Phys. A **50**, 095002 (2017).
[37] M. Serbyn, Z. Papić, and D. A. Abanin, Thouless energy and multifractality across the many-body localization transition, Phys. Rev. B **96**, 104201 (2017).
[38] M. Schiulaz, E. J. Torres-Herrera, and L. F. Santos, Thouless and relaxation time scales in many-body quantum systems, Phys. Rev. B **99**, 174313 (2019).
[39] R. Vosk, D. A. Huse, and E. Altman, Theory of the Many-Body Localization Transition in One-Dimensional Systems, Phys. Rev. X **5**, 031032 (2015).
[40] A. C. Potter, R. Vasseur, and S. A. Parameswaran, Universal Properties of Many-Body Delocalization Transitions, Phys. Rev. X **5**, 031033 (2015).
[41] D. A. Abanin, J. H. Bardarson, G. De Tomasi, S. Gopalakrishnan, V. Khemani, S. A. Parameswaran, F. Pollmann, A. C. Potter, M. Serbyn, and R. Vasseur, Distinguishing localization from chaos: Challenges in finite-size systems, Ann. Phys. **427**, 168415 (2021).
[42] A. Pal and D. A. Huse, Many-body localization phase transition, Phys. Rev. B **82**, 174411 (2010).
[43] M. L. Mehta, *Random Matrices* (Elsevier, Amsterdam, 2004).
[44] D. J. Luitz, N. Laflorencie, and F. Alet, Many-body localization edge in the random-field Heisenberg chain, Phys. Rev. B **91**, 081103(R) (2015).
[45] W. De Roeck, F. Huveneers, M. Müller, and M. Schiulaz, Absence of many-body mobility edges, Phys. Rev. B **93**, 014203 (2016).
[46] M. Akila, D. Waltner, B. Gutkin, and T. Guhr, Particle-time duality in the kicked Ising spin chain, J. Phys. A **49**, 375101 (2016).
[47] B. Bertini, P. Kos, and T. Prosen, Exact Spectral form Factor in a Minimal Model of Many-Body Quantum Chaos, Phys. Rev. Lett. **121**, 264101 (2018).
[48] M. Sonner, A. Lerose, and D. A. Abanin, Characterizing many-body localization via exact disorder-averaged quantum noise, arXiv:2012.00777.
[49] A. Lerose, M. Sonner, and D. A. Abanin, Influence Matrix Approach to Many-Body Floquet Dynamics, Phys. Rev. X **11**, 021040 (2021).
[50] See Supplemental Material at http://link.aps.org/supplemental/10.1103/PhysRevB.104.L081112 for a description of the transfer matrix approach to SFF, for a discussion of fits to the spectral function, and for a detailed comparison of the Thouless energy extracted from SFF and from the spectral function.
[51] F. Haake, *Quantum Signatures of Chaos* (Springer, Berlin, 2006).
[52] V. Oganesyan and D. A. Huse, Localization of interacting fermions at high temperature, Phys. Rev. B **75**, 155111 (2007).
[53] L. D'Alessio and M. Rigol, Long-Time Behavior of Isolated Periodically Driven Interacting Lattice Systems, Phys. Rev. X **4**, 041048 (2014).
[54] E. Brézin and S. Hikami, Spectral form factor in a random matrix theory, Phys. Rev. E **55**, 4067 (1997).
[55] S. J. Garratt and J. T. Chalker, Local Pairing of Feynman Histories in Many-Body Floquet Models, Phys. Rev. X **11**, 021051 (2021).
[56] D. J. Luitz and Y. Bar Lev, Anomalous Thermalization in Ergodic Systems, Phys. Rev. Lett. **117**, 170404 (2016).
[57] A. B. Harris, Effect of random defects on the critical behaviour of Ising models, J. Phys. C **7**, 1671 (1974).
[58] A. Chandran, C. R. Laumann, and V. Oganesyan, Finite size scaling bounds on many-body localized phase transitions, arXiv:1509.04285.
[59] J. Wuttke, Laplace-Fourier transform of the stretched exponential function: Analytic error bounds, double exponential transform, and open-source implementation "libkww," Algorithms **5**, 604 (2012).
[60] K. Agarwal, E. Altman, E. Demler, S. Gopalakrishnan, D. A. Huse, and M. Knap, Rare-region effects and dynamics near the many-body localization transition, Ann. Phys. (Berlin, Ger.) **529**, 1600326 (2017).
[61] S. J. Garratt and J. T. Chalker, Many-Body Delocalization as Symmetry Breaking, Phys. Rev. Lett. **127**, 026802 (2021).

Supplemental Material for "Thouless Energy across Many-Body Localization Transition in Floquet Systems"

Michael Sonner,[1] Maksym Serbyn,[2] Zlatko Papić,[3] and Dmitry A. Abanin[1]

[1] *Department of Theoretical Physics, University of Geneva, 24 quai Ernest-Ansermet, 1211 Geneva, Switzerland*
[2] *IST Austria, Am Campus 1, 3400 Klosterneuburg, Austria*
[3] *School of Physics and Astronomy, University of Leeds, Leeds LS2 9JT, United Kingdom*

(Dated: June 7, 2021)

In this Supplemental Material, we provide additional details on the calculation of spectral form factor using the transfer matrix. In addition, we discuss the fitting procedure for spectral function and also discuss its properties at the localization transition.

I. SPECTRAL FORM FACTOR FROM TRANSFER MATRICES

Spectral Form Factors are a non self-averaging quantity [R1] and thus manually averaging over disorder realizations can be difficult and require many samples. In order to check whether the oscillations observed at short times in Fig. 1(c) are due to lack of disorder averaging or reflect physical behavior of $K(\tau)$, we employ a dual transfer matrix approach [R2, R3] to calculate $K(\tau)$ for small τ. We start from the spectral form factor Eq. (2) expressed as the absolute square of the trace over the Floquet operator $\hat{F}$ in Eq. (1) raised to the power τ, and express it as a single trace of a operator $\hat{U}^\tau$ acting in a doubled Hilbert space:

$$K(\tau) = |\mathrm{Tr}(\hat{F}^\tau)|^2 = \mathrm{Tr}(\hat{F}^\tau \otimes \hat{F}^{-\tau}) = \mathrm{Tr}(\hat{U}^\tau). \tag{S1}$$

This can be interpreted as a partition function of a 2D Ising model with complex coefficients [R2] or as a contraction of a tensor network [R3]. The Floquet operator is in this language a transfer matrix, facilitating the contraction of the tensor network in the time-like direction. It is also possible however, to contract the tensor network in the spatial direction. This introduces a dual transfer matrix $\tilde{U}_i$ which acts on a $2^{2\tau}$ dimensional Hilbert space which represent the spins of site i at different times on two different branches σ_t and $\bar{\sigma}_t$:

$$\tilde{U}_i = \exp\left(i\sum_{t=1}^{\tau}(\tilde{J}\sigma_t^z\sigma_{t+1}^z - \tilde{J}^*\bar{\sigma}_t^z\bar{\sigma}_{t+1}^z + h_i\sigma_t^z - h_i^*\bar{\sigma}_t^z)\right)\exp\left(i\sum_{t=1}^{\tau}(\tilde{g}\sigma_t^x - \tilde{g}^*\bar{\sigma}_t^x + \eta - \tilde{\eta})\right), \tag{S2}$$

where we introduced the following notations:

$$\tilde{J} = -\frac{\pi}{4} - i\log\tan g, \quad \tilde{g} = \arctan(ie^{-iJ}), \quad \eta = -\frac{i\pi}{4} + \frac{1}{2}\log(\sin(g)\cos(g)), \quad \tilde{\eta} = -\frac{i\pi}{4} + \frac{1}{2}\log(\sin(\tilde{g})\cos(\tilde{g})). \tag{S3}$$

In both branches, the boundary conditions are periodic $\sigma_0 = \sigma_t$. This representation has the advantage that disorder averaging of the SFF can now be performed explicitly [R3, R4] by using that $\int \frac{\mathrm{d}xh}{2\pi}\exp(ih\sum_{\tau=0}^{T}\sigma^\tau - \bar{\sigma}^\tau) = \delta(\sum_\tau^t \sigma_\tau - \bar{\sigma}_\tau)$. This leaves us with expression

$$\langle K(\tau)\rangle = \mathrm{Tr}(\tilde{U}^L P), \tag{S4}$$

where P is the projection on the sector defined by $\sum_\tau^t \sigma_\tau = \sum_\tau^t \bar{\sigma}_\tau$. Computation can be made more efficient by utilizing the tensor product structure of $\tilde{U}$ and implementing the projection operator by just summing over entries which are allowed by the constraint in order to compute the trace. We used this approach to compute data points for short times in Fig. 1(c) in the main text.

II. FITS TO THE SPECTRAL FUNCTION

Previous work reported stretched exponential decay of connected correlation functions in the model considered here [R5]. Since the spectral function is the Fourier transform of the real time correlation function, we use the Kohlrausch-William-Watts (KWW) function for fitting. The KWW function $Q_\beta(\omega)$ corresponds to the cosine Fourier

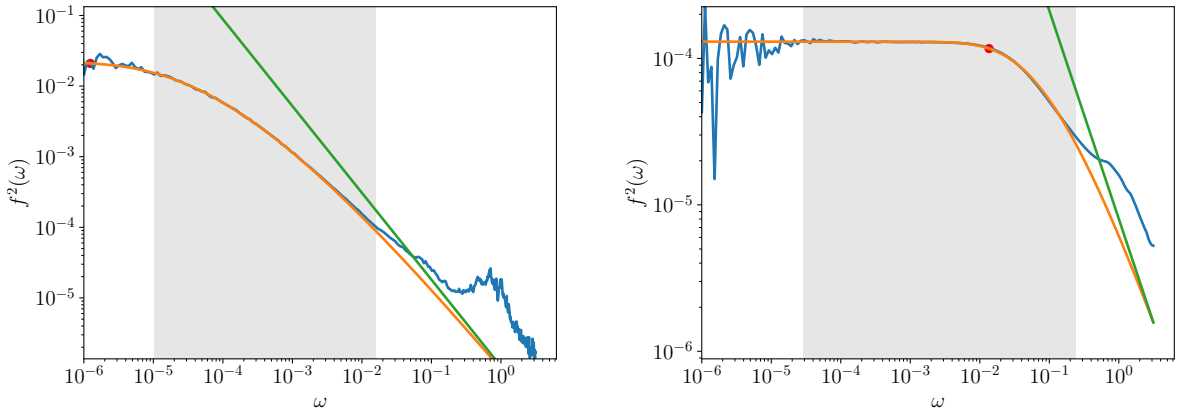

FIG. S1. Spectral function $f^2(\omega)$ fitted with the Fourier transform of a stretched exponential for two different parameters: $L = 14; g/\frac{\pi}{4} = 0.45$ and $L = 14; g/\frac{\pi}{4} = 0.70$. The shaded interval indicates the fitting region. The red dot indicates the inflection point which can be taken as Thouless' energy. The asymptotic power law is indicated as green line.

transform of the stretched exponential function e^{-t^β} and is implemented using the Python package [R6]. We choose the boundaries for the fit to exclude the peak at frequencies of the order of one that stems from local physics as well as low-frequency noise, see dashed lines in Fig. S1 for illustration. We parametrize the fitting function by three parameters, as $cQ_\beta(\omega/\Omega)$, where c sets the overall scale, Ω sets the energy scale, and β corresponds to the power in stretched exponential. Parameters c, Ω, and β are determined using the `curve_fit` routine from the `scipy` package.

We define the Thouless energy as the inflection point of the fitted function $cQ_\beta(\omega/\Omega)$, which matches well with the onset of the decay, see Fig. S1 for examples. The asymptotic power law decay of this function is determined by the stretched exponential exponent β. We note that this asymptotic power law decay corresponds to large frequencies, and thus for the weak disorder case falls outside of the fitting region. The covariance matrix entries however show that the fit still works even for relatively low disorder.

III. SPECTRAL FUNCTION VS SPECTRAL FORM FACTOR

The Thouless energy extracted from the spectral function strongly depends on the exact methodology especially in the strongly disordered regime where the spectral function is flat. However, by comparing the spectral function to the spectral form factor in Fig. S2 we can see that both methods qualitatively agree with each other. To establish this further, we compare the scaling of the Thouless time with system size in Fig. S3. On the ergodic side, we expect Thouless time to become a constant of order inverse bandwith, while it scales exponentially near the transition. This behavior can be observed in both approaches.

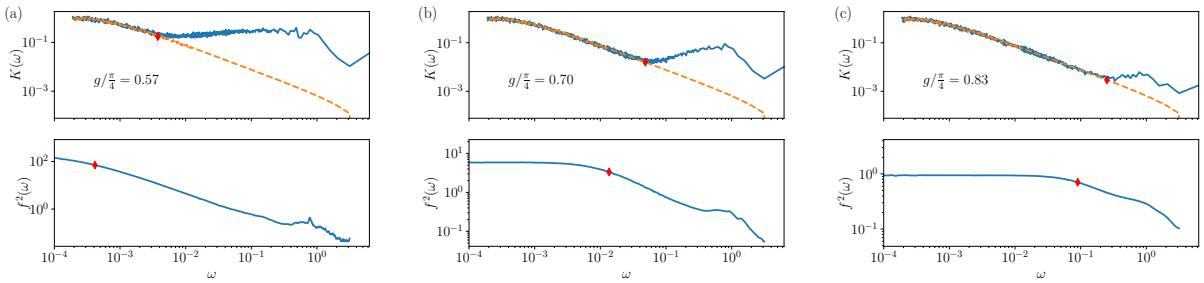

FIG. S2. Comparison of the spectral form factor (upper panels) with the spectral function (lower panels). The estimated Thouless energy from each of the two methods is marked with a red diamond.

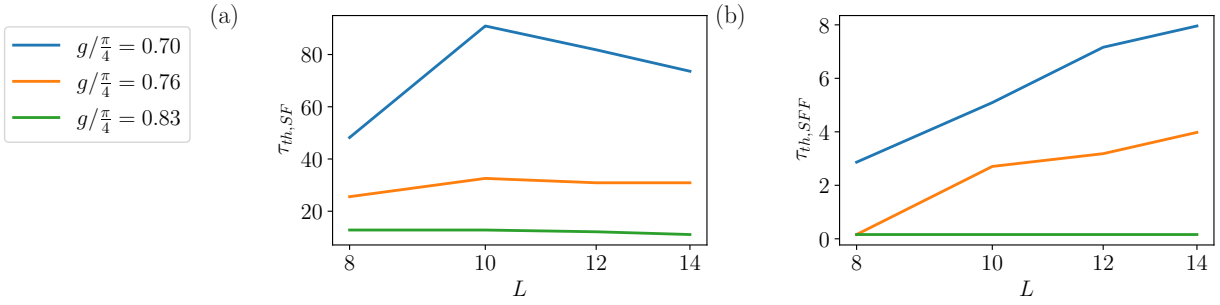

FIG. S3. Thouless time vs system size from the spectral function (left) and the spectral form factor (right). With both definitions, Thouless time increases strongly with system size.

IV. SPECTRAL FUNCTION AT THE MBL TRANSITION

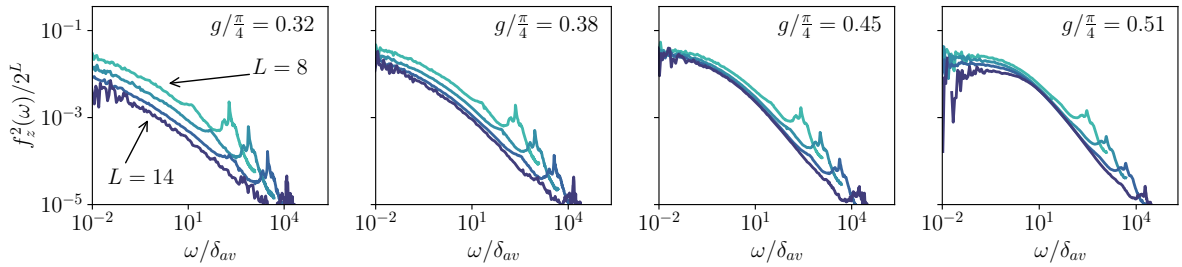

FIG. S4. Spectral function divided by Hilbert space dimension plotted as energy divided by the average level spacing across the MBL transition. With this scaling the functions for different lengths collapse at the transition point $g/\frac{\pi}{4} = 0.45$ for low frequencies.

The low frequency behavior of the spectral function is governed by only two energy scales: the average many body level spacing δ_{av} and Thouless' energy E_{Th}. At the MBL transition, those two scales were suggested to coincide [R7–R9]. Thus it is natural to assume that the system size scaling to be of the form

$$f(\omega, L) = C(L) f_* \left(\frac{\omega}{\delta(L)} \right). \tag{S5}$$

Using the zero frequency limit on the ergodic side, $\lim_{\omega \to 0} f(\omega, L) = 2^L$, we fix the constant

$$C(L) = 2^{-L}, \tag{S6}$$

which suggest the collapse of $2^{-L} f\left(\omega/\delta(L)\right)$. Indeed, in Fig. S4 we observe that with this scaling, the low frequency part of the spectral function collapses at the transition point. This can potentially be utilised as a sensitive criterion for the MBL transition for small system sizes.

[R1] R. E. Prange, The spectral form factor is not self-averaging, Phys. Rev. Lett. **78**, 2280 (1997).

[R2] M. Akila, D. Waltner, B. Gutkin, and T. Guhr, Particle-time duality in the kicked ising spin chain, Journal of Physics A: Mathematical and Theoretical **49**, 375101 (2016).

[R3] B. Bertini, P. Kos, and T. c. v. Prosen, Exact spectral form factor in a minimal model of many-body quantum chaos, Phys. Rev. Lett. **121**, 264101 (2018).

[R4] M. Sonner, A. Lerose, and D. A. Abanin, Characterizing many-body localization via exact disorder-averaged quantum noise (2020), arXiv:2012.00777 [cond-mat.dis-nn].

[R5] T. L. M. Lezama, S. Bera, and J. H. Bardarson, Apparent slow dynamics in the ergodic phase of a driven many-body localized system without extensive conserved quantities, Phys. Rev. B **99**, 161106 (2019).

[R6] J. Wuttke, Laplace–fourier transform of the stretched exponential function: Analytic error bounds, double exponential transform, and open-source implementation "libkww", Algorithms **5**, 604 (2012).
[R7] R. Vosk, D. A. Huse, and E. Altman, Theory of the many-body localization transition in one-dimensional systems, Phys. Rev. X **5**, 031032 (2015).
[R8] A. C. Potter, R. Vasseur, and S. A. Parameswaran, Universal properties of many-body delocalization transitions, Phys. Rev. X **5**, 031033 (2015).
[R9] M. Serbyn, Z. Papić, and D. A. Abanin, Criterion for many-body localization-delocalization phase transition, Phys. Rev. X **5**, 041047 (2015).